

# 2D and 3D topological phases in BiTeX compounds

S. V. Eremeev,<sup>1,2,3,4</sup> I. A. Nechaev,<sup>5,1,2</sup> and E. V. Chulkov<sup>5,1,2,4,6</sup>

<sup>1</sup>*Tomsk State University, 634050 Tomsk, Russia*

<sup>2</sup>*Saint Petersburg State University, 198504 Saint Petersburg, Russia*

<sup>3</sup>*Institute of Strength Physics and Materials Science, 634055 Tomsk, Russia*

<sup>4</sup>*Donostia International Physics Center, 20018 San Sebastián/Donostia, Spain*

<sup>5</sup>*Centro de Física de Materiales CFM - MPC and Centro Mixto CSIC-UPV/EHU, 20018 San Sebastián/Donostia, Spain*

<sup>6</sup>*Departamento de Física de Materiales UPV/EHU, Facultad de Ciencias Químicas, UPV/EHU, Apdo. 1072, 20080 San Sebastián/Donostia, Spain*

(Dated: March 15, 2022)

Recently, it was shown that quantum spin Hall insulator (QSHI) phase with a gap wide enough for practical applications can be realized in the ultra thin films constructed from two inversely stacked structural elements of trivial band insulator BiTeI. Here, we study the edge states in the free-standing Bi<sub>2</sub>Te<sub>2</sub>I<sub>2</sub> sextuple layer (SL) and the electronic structure of the Bi<sub>2</sub>Te<sub>2</sub>I<sub>2</sub> SL on the natural BiTeI substrate. We show that the topological properties of the Bi<sub>2</sub>Te<sub>2</sub>I<sub>2</sub> SL on this substrate keep  $\mathbb{Z}_2$  invariant. We also demonstrate that ultra thin centrosymmetric films constructed in the similar manner but from related material BiTeBr are trivial band insulators up to five-SL film thickness. In contrast to Bi<sub>2</sub>Te<sub>2</sub>I<sub>2</sub> for which the stacking of nontrivial SLs in 3D limit gives a strong topological insulator (TI) phase, strong TI is realized in 3D Bi<sub>2</sub>Te<sub>2</sub>Br<sub>2</sub> in spite of the SL is trivial. For the last material of the BiTeX ( $X=\text{I,Br,Cl}$ ) series, BiTeCl, both 2D and 3D centrosymmetric phases are characterized by topologically trivial band structure.

PACS numbers: 71.15.-m, 71.18.+y, 73.22.-f

## I. INTRODUCTION

Starting from the theoretical predictions by Kane and Mele<sup>1</sup> and Bernevig et al.<sup>2,3</sup>, the  $\mathbb{Z}_2$  two-dimensional topological insulator (2D TI) or the QSHI phase, in which spin-helical gapless edge states counter-propagate along the boundary with opposite spins, providing quantum spin Hall effect (QSHE)<sup>1</sup> with quantized spin-Hall conductance, attract considerable attention of researchers. After experimental observations of the QSHE in HgTe/CdTe and InAs/GaSb quantum wells,<sup>4,5</sup> a number of 2D TIs were theoretically proposed.<sup>6</sup> These proposals were mainly based on the layers of bismuth, graphene, or heavy elements analogs of graphene, implying the gap tuning by strain, adatoms deposition, chemical functionalization, growing on substrates, or sandwiching. In contrast to 3D TIs, for which the existence of topologically protected Dirac surface states was found in a wide variety of materials, the edge states in 2D TIs by now were directly observed experimentally in a limited number of systems like Bi(111)-bilayer islands on a Bi-crystal surface<sup>7</sup>, in Bi(110)<sup>8</sup> and Sb(111)<sup>9</sup> thin films, and step edges in ZrTe<sub>5</sub>,<sup>10,11</sup> while the QSHE was confirmed in the quantum wells with tiny band gaps only,<sup>6</sup> where a topologically protected state does not survive at temperatures above 10 K. Thus, the goal that remains to be actual so far is to search for robust and easily fabricated new 2D TIs with a sufficiently large band gap providing edge states accessible to experimental probes at room temperature.

Recently, it was suggested a distinct way to design novel topological systems on the base of two-dimensional materials consisting of layered band insulators.<sup>12</sup> It was

demonstrated that these systems can be realized under normal conditions in thin films comprising van-der-Waals coupled structure elements (trilayers, TLs) of the giant-Rashba semiconductor BiTeI, which belongs to the intensively investigated chalcogenides BiTeX ( $X=\text{Cl, Br, and I}$ ).<sup>13-29</sup>

BiTeX compounds have a hexagonal non-centrosymmetric crystal structure built of ionically-bonded X-Bi-Te TL stacked along the hexagonal  $z$  axis. In addition to the large bulk and surface Rashba splitting in these materials, a single BiTeX trilayer holds the giant Rashba-split states as well.<sup>30</sup> Among BiTeX materials, BiTeI demonstrate the largest bulk Rashba splitting, while BiTeCl stands out for its isotropic spin-split metallic surface state lying deep inside the bulk band gap, which is the biggest one in the BiTeX series. Generally, the BiTeX surfaces, which can be Te- or X-terminated, can possess, respectively, electron- or hole-like Rashba-split surface states that emerge by splitting off from the lowest conduction (highest valence) band, owing to the negative (positive) surface potential bending.<sup>14</sup> However, it turned out that the surface of BiTeI obtained by natural cleavage of single crystals grown by the Bridgman method always hold both types of the surfaces states due to two different type domains (Te- and I-terminated), inhomogeneously distributed over the surface.<sup>15,16,23,24,26,27,29</sup> These surface domains are the consequence of a large number of randomly distributed bulk stacking faults, in which the TLs stacking order is inverted.<sup>26,27,29</sup> The calculated bulk stacking fault formation energy in the BiTeI bulk, 1 meV, is much smaller than for BiTeBr (46 meV) and BiTeCl (60 meV)<sup>27</sup> that explains the existence of

the mixed domain termination on the BiTeI surface in contrast to the BiTeBr and BiTeCl (0001) surfaces characterized by single polar domains.

It was demonstrated<sup>12</sup> that a centrosymmetric sextuple layer (SL) constructed from two BiTeI TLs with facing Te-layer sides is a 2D TI with the inverted gap of about 60 meV at  $\bar{\Gamma}$ , which is sufficiently enough for room temperature spintronics applications. The gap inversion occurs due to the bonding-antibonding splitting between one of the Te-related valence bands (VBs) and one of the conduction bands (CBs) formed by Bi orbitals. The films of a several SL thickness demonstrate rapid decrease in the gap width with the number of SLs along with oscillating behavior in  $\mathbb{Z}_2$  topological invariant like in thin films of the Bi<sub>2</sub>Te<sub>3</sub> family (see, e.g., Refs. 31–34). The corresponding bulk system composed of SLs turned out to be a strong 3D TI (hereafter referred to as Bi<sub>2</sub>Te<sub>2</sub>I<sub>2</sub>). It is energetically unfavourable by only 0.5 meV compared with the non-centrosymmetric BiTeI. It should be noted that due to the stacking faults mentioned above crystals of BiTeI grown by the Bridgman method already contain the desired SLs, and that the inverted stacking can be experimentally observed and controllably manufactured.

Most of earlier theoretically predicted 2D TIs were considered as free-standing systems. However, for practical applications, a freestanding 2D TI must be placed or grown on appropriate substrate which, in general, will influence the intrinsic topological properties of thin films due to interfacial and proximity effects<sup>35</sup> such as mismatch in the lattice constants and charge transfer at the interface of diverse materials.<sup>36–38</sup> Therefore, suitable substrates to support room-temperature TIs are important for potential device applications. Several 2D TI systems, mostly Bi-based layers on silicon (or SiC) substrate were theoretically suggested.<sup>39–45</sup> However, they have not been experimentally realized up to now. The exception is the honeycomb Bi on Au/Si(111)-( $\sqrt{3}\times\sqrt{3}$ ) substrate structure, which was successfully grown as confirmed by LEED and STM measurements.<sup>45</sup> Nevertheless, the QSHE has not been proved to be observable in this system so far. In this regard, the Bi<sub>2</sub>Te<sub>2</sub>I<sub>2</sub>-SL 2D TI has a significant advantage, since it has a natural substrate – the non-centrosymmetric BiTeI band insulator, which guarantees an absence of both lattice mismatch and interface charge transfer effects, since there is no work function difference between the substrate and the 2D TI adlayer.

In this paper, using first-principles electronic structure calculations, we examine the edge states of the Bi<sub>2</sub>Te<sub>2</sub>I<sub>2</sub> 2D TI of one-SL thickness for different edge orientations. We also consider the effect of the BiTeI substrate on the electronic structure of this 2D TI. Finally, we study the topological properties of the related 2D and 3D centrosymmetric phases Bi<sub>2</sub>Te<sub>2</sub>Br<sub>2</sub> and Bi<sub>2</sub>Te<sub>2</sub>Cl<sub>2</sub>.

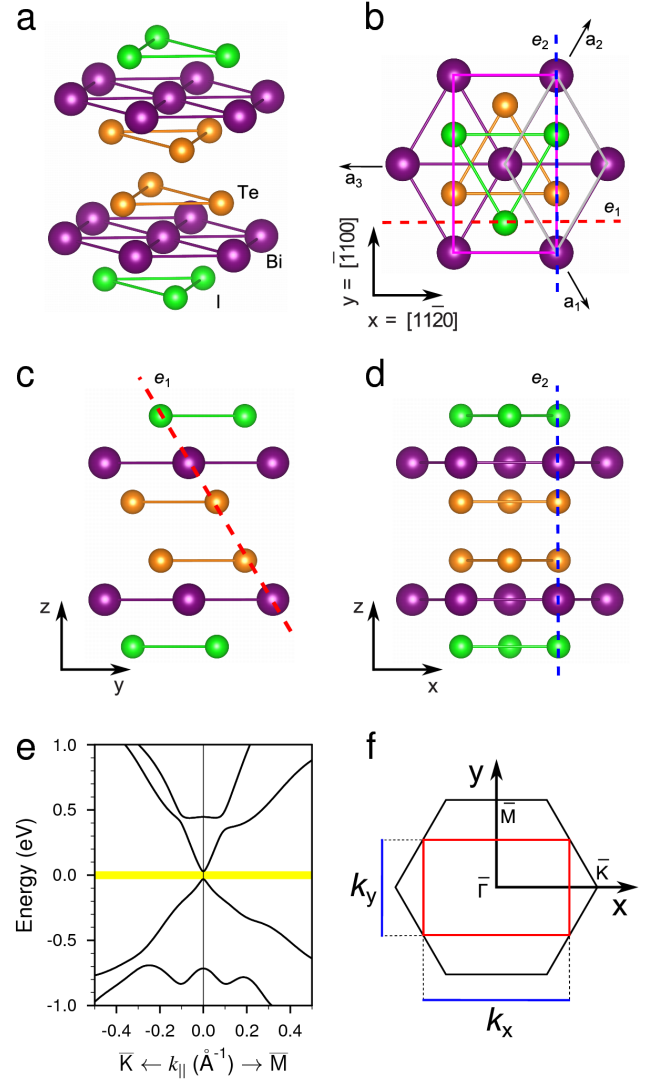


FIG. 1. Atomic structure of the Bi<sub>2</sub>Te<sub>2</sub>I<sub>2</sub> one-SL film (a) with its top view (b) and side views in  $y-z$  and  $x-z$  planes (c and d, respectively).  $e_1$  and  $e_2$  dashed lines (red and blue, respectively) show cleavage planes for considered stoichiometric edges. Light-gray rhombus and magenta rectangle in (b) mark the unit cell and related rectangular cell by repeating of which in  $x$  or  $y$  direction we construct different nanoribbons. (e) Band structure of the free-standing Bi<sub>2</sub>Te<sub>2</sub>I<sub>2</sub> SL along  $\bar{\Gamma}-\bar{K}$  and  $\bar{\Gamma}-\bar{M}$  directions of the 2D hexagonal Brillouin zone (BZ); yellow stripe shows the region of the band inverted gap. Black hexagon in (f) shows 2D hexagonal BZ; red rectangle shows 2D BZ for rectangular cell and blue lines indicate its projections onto 1D BZs along  $k_x$  and  $k_y$  axes.

## II. METHODS

Calculations were carried out within generalized gradient approximation (GGA) with the projector augmented-wave method<sup>46,47</sup> as realized in the Vienna Ab Initio Simulation Package (VASP).<sup>48,49</sup> DFT-D3 van der Waals (vdW) correction<sup>50</sup> was applied for accurate structure

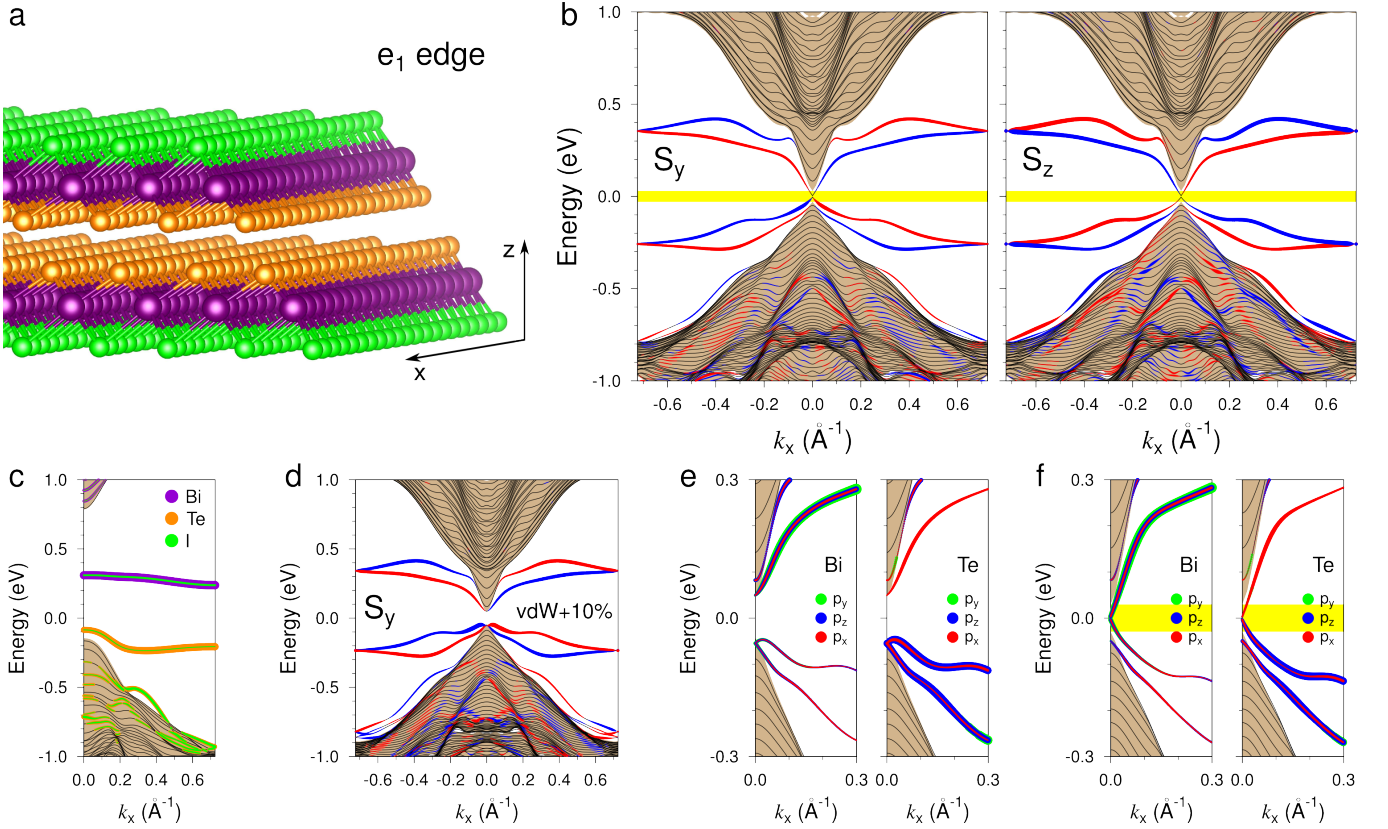


FIG. 2. (a) Atomic structure of the  $e_1$  edge. (b) Electronic spectrum and spin polarization for localized states at the edge; red/blue circles represent positive/negative sign of the spin component for localized states. (c) Atom-projected localization of the trivial dangling bond states as calculated with the switched off SOC. (d) Electronic structure of the  $e_1$  edge of the topologically trivial  $\text{Bi}_2\text{Te}_2\text{I}_2$  film with vdW spacing expanded by 10%. Orbital character of the localized states for Bi (left panel) and Te (right panel) contributions for the trivial (vdW+10%) system (e) and the  $\text{Bi}_2\text{Te}_2\text{I}_2$  QSH insulator (f).

optimization. Bulk lattice parameters and atomic positions of  $\text{Bi}_2\text{Te}_2X_2$  phases (the 164 ( $\text{P}\bar{3}\text{m}1$ ) space group) were optimized. The optimized  $a$  and  $c$  parameters for  $\text{Bi}_2\text{Te}_2\text{I}_2$  bulk have been obtained to equal 4.354 and 13.421 Å, respectively, and they were found to be 4.474 and 11.676 Å and 4.288 and 12.155 Å for  $\text{Bi}_2\text{Te}_2\text{Br}_2$  and  $\text{Bi}_2\text{Te}_2\text{Cl}_2$ , respectively. For all  $\text{Bi}_2\text{Te}_2X_2$  bulk phases, the  $a$  parameter is slightly larger than that in respective non-centrosymmetric  $\text{BiTeX}$  compounds. The Bi-Te and Bi- $X$  interlayer spacings in  $\text{Bi}_2\text{Te}_2X_2$  bulk are also close to those in  $\text{BiTeX}$ ; Te-Te( $X$ - $X$ ) interlayer distances in  $\text{Bi}_2\text{Te}_2X_2$  bulk phases vary in the range of  $X=\text{I}, \text{Br}, \text{Cl}$  as 2.655(3.094), 2.456(2.521), and 2.796(2.623) Å. For single free-standing  $\text{Bi}_2\text{Te}_2X_2$  SLs, we performed additional structural optimization. A small contraction was obtained in the Te-Te distance, and a small expansion was found in the outer Bi- $X$  spacing, while Te-Bi interlayer spacing remained unchanged as compared to the respective bulk values. The  $\mathbb{Z}_2$  topological invariant was calculated by using the method based on tracking the evolution of hybrid Wannier functions realized in Z2Pack<sup>51</sup>.

### III. RESULTS AND DISCUSSION

#### A. Edge states in $\text{Bi}_2\text{Te}_2\text{I}_2$ -SL nanoribbons

First we studied the energies of edges with different geometry to find out the most stable edge for the  $\text{Bi}_2\text{Te}_2\text{I}_2$ -SL nanoribbon. We have considered stoichiometric mutually perpendicular cleavage planes  $e_1$  and  $e_2$ , see Fig 1(b-d). The  $e_1$  plane is parallel to the  $[\bar{1}100]$  ( $x$ ) axis and crosses (0001) ( $xy$ ) plane at an angle of  $56.96^\circ$ . The  $e_2$  plane is parallel to the  $[11\bar{2}0]$  ( $y$ ) axis and passes perpendicular to the (0001) plane. As expected from the effective continuous model,<sup>52</sup> the decay depth of the topological edge states in 2D TI should be much larger than that for the Dirac surface states in 3D TI. Consequently, to avoid the finite size effect, the nanoribbon width should be chosen as large as possible. We have constructed nanoribbons bounded by the two parallel  $e_1$  and  $e_2$  cleavage planes of the width of  $\sim 150$  Å. We found that the  $e_1$  edge is by  $\sim 170$  meV/Å<sup>2</sup> more favorable than the  $e_2$  one. The stability of the  $e_1$  edge looks reasonable, because the preferred cleavage plane is the one, which minimizes the number of broken bonds. The square of

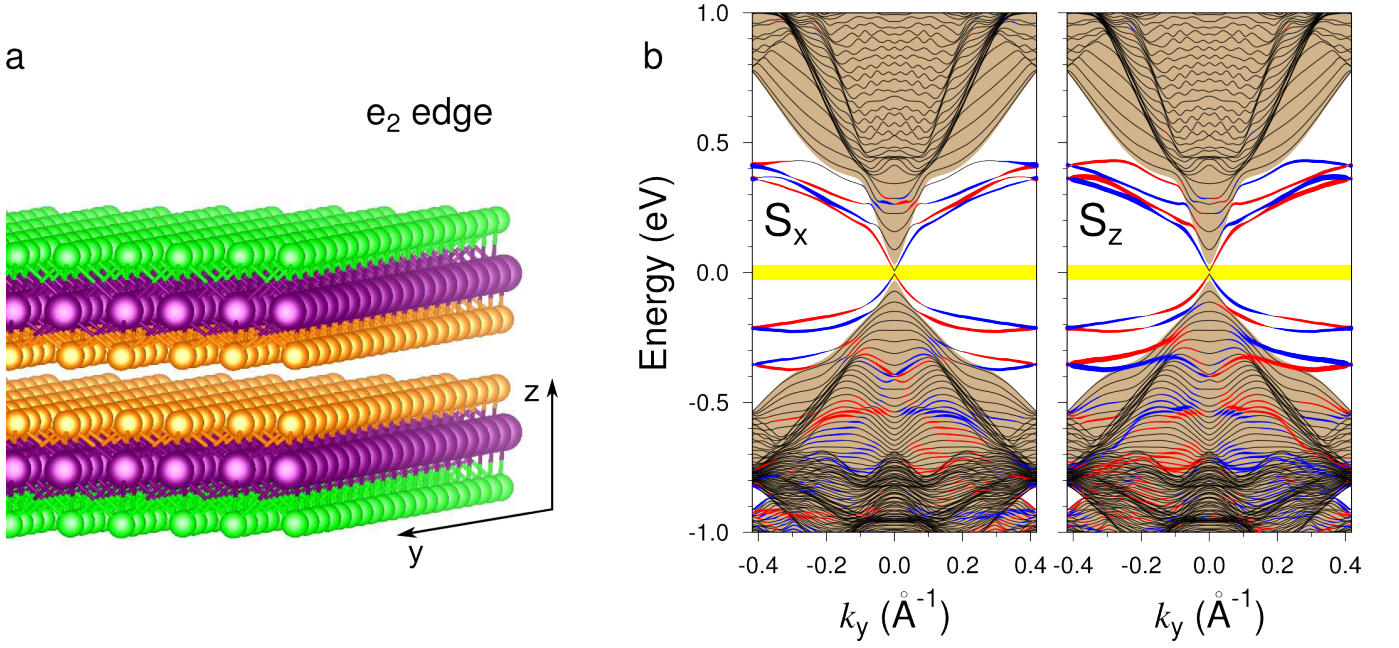


FIG. 3. Atomic structure (a) and electronic spectrum with spin polarization (b) for the  $e_2$  edge of  $\text{Bi}_2\text{Te}_2\text{I}_2$  nanoribbon.

the  $e_1$  plane is about 1.5 times smaller than that of the  $e_2$  plane, while the number of broken bonds at the  $e_2$  plane is two times bigger as compared to  $e_1$  (8 and 4, respectively), and thus the density of the broken bonds (per unit square) is smaller for the  $e_1$  edge. Note that the stoichiometric cleavage plane, similar to  $e_1$  was found to be stable for the  $\text{Bi}_2\text{Te}(\text{Se})_3$  single quintuple layer (QL).<sup>53</sup>

Next, we examine the electronic structure of the ribbons with the  $e_1$  and  $e_2$  edges. Fig. 1(e) shows the spectrum of the  $\text{Bi}_2\text{Te}_2\text{I}_2$  film of single SL thickness calculated along high-symmetry directions of the hexagonal Brillouin zone [Fig. 1(f)]. As was demonstrated in Ref. 12 this film has an inverted gap of  $\sim 60$  meV at the Fermi level, and in this gap (yellow stripe) we expect to find one-dimensional topological spin-helical states localized at the edge of the nanoribbon. When the  $e_1$  ( $e_2$ ) edge is formed, the 2D BZ of the  $\text{Bi}_2\text{Te}_2\text{I}_2$ -SL is projected onto 1D BZ along the  $k_x$  ( $k_y$ ) direction [Fig. 1(f)].

The calculated electronic structure of the  $e_1$  ribbon (Fig. 2(a)) is shown in Fig. 2(b), where left and right panels demonstrate the same electronic spectrum but different projections of the spin expectation value for the localized states,  $S_y$  and  $S_z$ , which are orthogonal to the wave vector  $k_x$  ( $S_x$  component of the spin is zero). They are calculated as a sum over atomic contributions from five near-edge atomic layers. As can be seen in Fig. 2(b), the spectrum has a gap at the Dirac point (of few meV) as the result of hybridization between edge states localized at the opposite edges of the ribbon despite we have chosen quite wide ribbon. Another observation is that beside the  $\bar{\Gamma}$  Dirac state the band structures also show the presence of a number of spin-polarized resonant states mainly in the valence band region as well as two triv-

ial Rashba-split dangling bond states in the gap region far from the  $\bar{\Gamma}$  point. These states are originated from the broken bonds at the edge. With switched off spin-orbit coupling (SOC) these dangling bond states appear as two almost dispersionless bands [Fig. 2(c)]. The occupied and unoccupied bands have an only small iodine contribution and the former band is mainly contributed by Te orbitals, while the latter is primarily formed by the Bi orbitals. Both bands have  $p_{yz}$  character over 1D BZ that reflects the fact the dangling bonds are oriented perpendicular to the  $e_1$  cleavage plane.

As was shown in Ref. 12, the vdW interaction between TLs that form the  $\text{Bi}_2\text{Te}_2\text{I}_2$ -SL is crucial to realize QSHI phase. The gap in the SL spectrum closes at increasing the vdW spacing by 5% and further increase in the vdW spacing reopens trivial gap. At 10% expansion, the spectrum has the trivial gap of the width comparable to that in the equilibrium band-inverted SL.<sup>12</sup> Constructing the nanoribbon with the vdW spacing expanded by 10%, we found merely two dangling bond states acquired the Rashba splitting (Fig. 2(d),  $S_y$  spin component is only shown). At large  $k_x$  ( $>0.3 \text{ \AA}^{-1}$ ) despite the spin splitting both bands keep their  $p_{yz}$  character, whereas at small  $k_x$  [Fig. 2(e)] the orbital character is changed due to emergence of  $p_x$  orbitals and the appearance of Bi  $p_{yx}$  states in the occupied band along with Te  $p_x$  states in the unoccupied band. Comparing the orbital character of the Rashba-split dangling bond states near the  $\bar{\Gamma}$  point at the edge in trivial (vdW-expanded) SL with that in the QSHI [Fig. 2(f)], one can conclude that the emergent Dirac states have the atom-type contributions and the orbital compositions similar to that of trivial states, with which the Dirac states hybridize strongly.



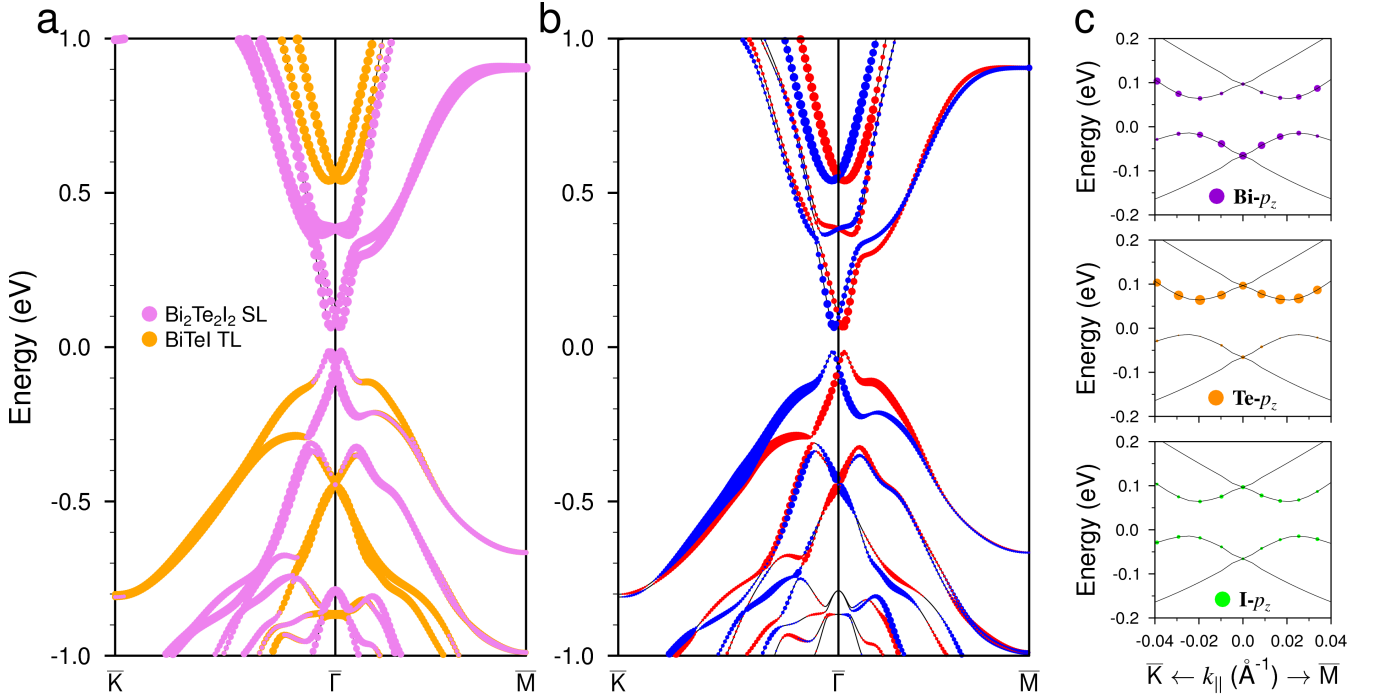


FIG. 4. Layer- (a) and spin-resolved (b) spectrum for  $\text{Bi}_2\text{Te}_2\text{I}_2$ -SL/ $\text{BiTeI}$ -TL film. (c) Orbital-resolved band structure in the vicinity of the  $\bar{\Gamma}$ -gap.

In the ribbon with the less stable  $e_2$  edge [Fig. 3(a)], the spectrum and different spin projections,  $S_x$  and  $S_z$  ( $S_y$  is zero in this case) of which are presented in Fig. 3(b), additional expected trivial Rashba-split dangling bond states are emerged in the projected gap. The number of such bands is two times larger as compared to the spectrum of the  $e_1$  edge owing to the fact that twice as many bonds break at the formation of this edge. However, as in the nanoribbon with  $e_1$  edge, the dangling bond states lie far from the  $\bar{\Gamma}$  gap region (yellow stripe) where topological Dirac state resides.

### B. $\text{Bi}_2\text{Te}_2\text{I}_2$ -SL 2D TI on $\text{BiTeI}$ band insulator substrate

As we pointed above, one of the main challenge for 2D TIs is appropriate substrate, and the advantage of  $\text{Bi}_2\text{Te}_2\text{I}_2$  is that it has a natural substrate –  $\text{BiTeI}$  band insulator, which guarantees the absence of both the lattice mismatch and the interface charge transfer effects. Since the charge transfer is mostly a local effect, we consider first the structure composed of  $\text{Bi}_2\text{Te}_2\text{I}_2$ -SL and a single  $\text{BiTeI}$  TL as  $[\text{I-Bi-Te-Te-Bi-I}]_{\text{SL}}-[\text{Te-Bi-I}]_{\text{TL}}$ . The calculated band spectrum of this structure is shown in Fig. 4. As can be seen in Fig. 4(a), the states forming a gap in this system belong to the  $\text{Bi}_2\text{Te}_2\text{I}_2$ -SL, while the states localized in the  $\text{BiTeI}$ -TL lie far from the gap edges, especially in the unoccupied part of the spectrum. Since the  $[\text{I-Bi-Te-Te-Bi-I}]_{\text{SL}}-[\text{Te-Bi-I}]_{\text{TL}}$  system lacks the inversion symmetry, the states possess the

Rashba spin-splitting (Fig. 4(b)). The splitting is almost isotropic with respect to  $k_{\parallel}$ , and splitting parameters are  $\Delta k=0.026(0.020) \text{ \AA}^{-1}$  and  $\Delta E=0.048(0.029) \text{ eV}$  for valence (conduction) band. Beside the gap in  $\text{Bi}_2\text{Te}_2\text{I}_2$  states acquires the Rashba splitting, its width becomes larger. In the free-standing inversion symmetric  $\text{Bi}_2\text{Te}_2\text{I}_2$  the gap is of 60 meV (Fig. 1(e)), and in  $[\text{I-Bi-Te-Te-Bi-I}]_{\text{SL}}-[\text{Te-Bi-I}]_{\text{TL}}$  the absolute gap  $E_g$  equals 78 meV (the  $\bar{\Gamma}$ -gap is  $E_g+\Delta E^{\text{VB}}+\Delta E^{\text{CB}}$ ). However, despite the Rashba splitting the gap-edge states remain inverted, as in the inversion symmetric  $\text{Bi}_2\text{Te}_2\text{I}_2$ .<sup>12</sup> In the vicinity of  $\bar{\Gamma}$ , the Bi  $p_z$ -orbitals mainly localized in the valence band, while Te  $p_z$  orbitals dominate in the lowest conduction band (Fig. 4(c)). The calculation of  $\mathbb{Z}_2$  for  $[\text{I-Bi-Te-Te-Bi-I}]_{\text{SL}}-[\text{Te-Bi-I}]_{\text{TL}}$  structure resulted in non-trivial topological invariant.

Next we increased the number of TLs in the slab so that the  $\text{BiTeI}$  part of the structure was sufficient to reproduce the  $\text{BiTeI}$  bulk. As in earlier works<sup>14,16,17</sup> we used  $\text{BiTeI}$  slab of 8 TLs thickness with the back, iodine-terminated, surface passivated by hydrogen. As can be seen in Fig. 5(a,b), in  $\text{Bi}_2\text{Te}_2\text{I}_2$ -SL@ $\text{BiTeI}$  heterostructure the  $\text{Bi}_2\text{Te}_2\text{I}_2$  states lie within the  $\text{BiTeI}$  bulk gap. The gap in  $\text{Bi}_2\text{Te}_2\text{I}_2$  states  $E_g=74 \text{ meV}$  is almost the same as in case of single TL  $\text{BiTeI}$  substrate but spin-splitting parameters became slightly smaller:  $\Delta k=0.018(0.014) \text{ \AA}^{-1}$  and  $\Delta E=0.030(0.018) \text{ eV}$  for valence (conduction) band. Such small alterations in the  $\text{Bi}_2\text{Te}_2\text{I}_2$  spectrum in the vicinity of  $\bar{\Gamma}$  do not affect the gap inversion as can be seen in Fig. 5(c). As before, the

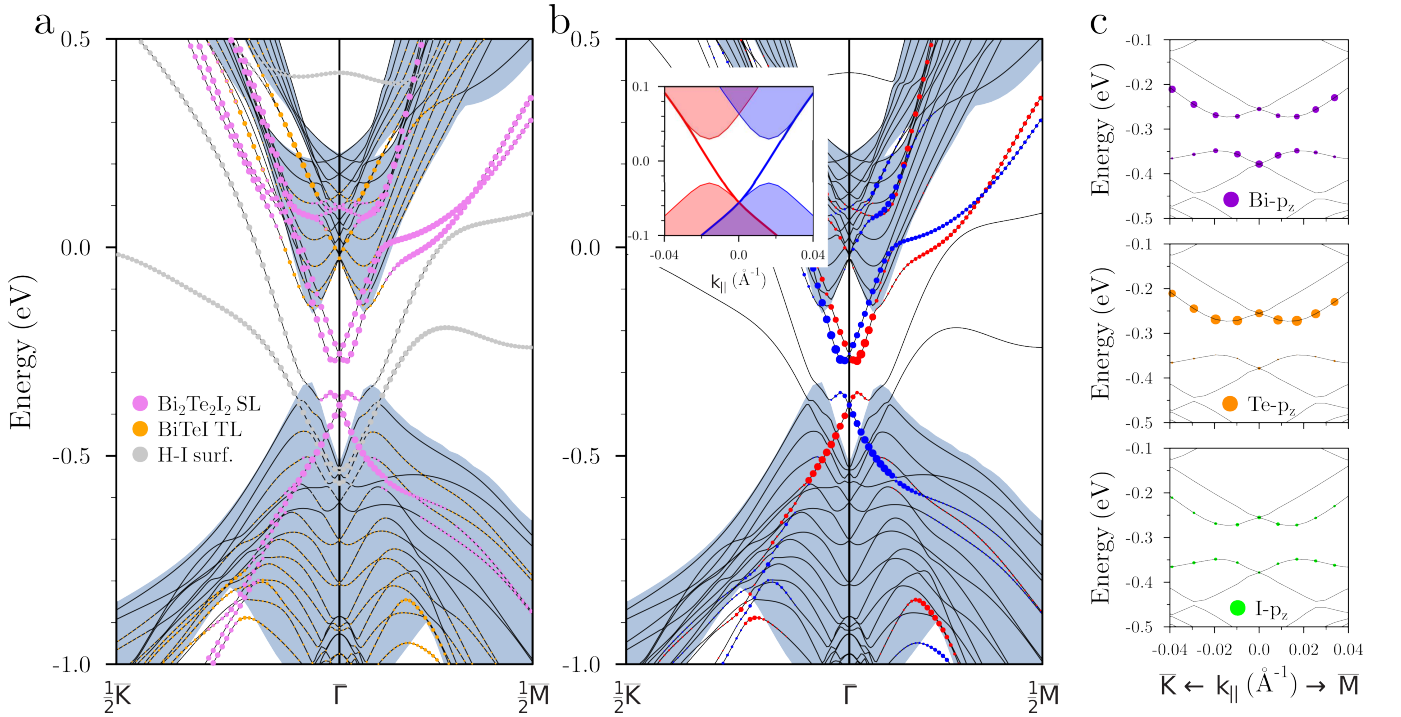


FIG. 5. Layer- (a) and spin-resolved (b) spectrum for  $\text{Bi}_2\text{Te}_2\text{I}_2\text{-SL@BiTeI}$  structure. (c) Orbital-resolved band structure in the vicinity of the  $\bar{\Gamma}$ -gap.

gap edges are mainly formed by  $p_z$  orbitals of Bi (VB) and Te (CB) atoms.

Thus, 2D TI  $\text{Bi}_2\text{Te}_2\text{I}_2$  survives on BiTeI substrate. This is due to the fact that  $\text{Bi}_2\text{Te}_2\text{I}_2$  and BiTeI are actually the same materials, which differ in TLs staking order only. It guarantees the absence of the interface potential because the interface  $[\text{I-Bi-Te-Te-Bi-I}]_{\text{SL}}\text{-}[\text{Te-Bi-I}]\text{-}[\text{Te-Bi-I}]\text{-}\dots$  can be regarded as the structure  $[\text{I-Bi-Te}]\text{-}[\text{Te-Bi-I}]\text{-}[\text{Te-Bi-I}]\text{-}[\text{Te-Bi-I}]\text{-}\dots$ , i.e., as the BiTeI surface, where uppermost TL has inverted atomic layer sequence. The splitting in the spin subbands in the 2D TI  $\text{Bi}_2\text{Te}_2\text{I}_2$  spectrum on the BiTeI substrate will result in the opposite  $k_{\parallel}$ -shifting of the corresponding spin branches of the Dirac state in the 1D spectrum as schematically shown in the inset in Fig. 5(b). Wherein, the Dirac point that is in the middle of the gap in the case of free-standing SL might be shifted downward to the region of the two-dimensional states.

### C. Search for 2D and 3D topological phases in $\text{Bi}_2\text{Te}_2\text{Br}_2$ and $\text{Bi}_2\text{Te}_2\text{Cl}_2$

Finally, we consider 2D and 3D centrosymmetric phases constructed from TLs of the related band insulators BiTeBr and BiTeCl. Despite the bulk stacking faults, which is a key element for centrosymmetric BiTeX phases, are missing in BiTeBr and BiTeCl obtained by the Bridgeman method as follows from the experiment<sup>27</sup> demonstrating the absence of the mixed-terminated sur-

faces in these materials, however, one can assume that centrosymmetric films of BiTeBr and BiTeCl can, in principle, be epitaxially grown.

Calculating the total energies of free-standing SLs of  $\text{Bi}_2\text{Te}_2\text{Br}_2$  and  $\text{Bi}_2\text{Te}_2\text{Cl}_2$  we found that they have lower (by 98 and 91 meV, respectively) energies than BiTeBr and BiTeCl films of double TL thickness have. However, the bulk phases composed of  $\text{Bi}_2\text{Te}_2\text{Br}_2$  and  $\text{Bi}_2\text{Te}_2\text{Cl}_2$  SLs are less favorable as compared to corresponding BiTeBr and BiTeCl non-centrosymmetric bulk crystals. The energy losing for  $\text{Bi}_2\text{Te}_2\text{Br}_2$  with respect to BiTeBr is 20.75 meV per BiTeI fu and it is 26.35 meV/fu for  $\text{Bi}_2\text{Te}_2\text{Cl}_2$  system in comparison with BiTeCl.

The band spectra of  $\text{Bi}_2\text{Te}_2\text{Br}_2$  and  $\text{Bi}_2\text{Te}_2\text{Cl}_2$  single, free-standing SLs [Fig. 6(a,b)], in general, are similar to that of  $\text{Bi}_2\text{Te}_2\text{I}_2$ , however, they have larger band gaps, 106 and 203 meV, respectively, and, according to  $\mathbb{Z}_2$  calculations, these centrosymmetric  $\text{Bi}_2\text{Te}_2\text{Br}_2$  and  $\text{Bi}_2\text{Te}_2\text{Cl}_2$  SLs are topologically trivial.

Next, like the case of  $\text{Bi}_2\text{Te}_2\text{I}_2$ , we addressed the electronic structure of the  $\text{Bi}_2\text{Te}_2\text{Br}_2$  and  $\text{Bi}_2\text{Te}_2\text{Cl}_2$  bulk. We revealed that  $\text{Bi}_2\text{Te}_2\text{Br}_2$  has an inverted band gap of 62 meV while  $\text{Bi}_2\text{Te}_2\text{Cl}_2$  bulk is a trivial band insulator with the gap of 92.5 meV and thus it is trivial in both 2D and 3D phases.

Considering the dependence of the  $\bar{\Gamma}$ -gap and the topological invariant on the film thickness for  $\text{Bi}_2\text{Te}_2\text{Br}_2$  and  $\text{Bi}_2\text{Te}_2\text{Cl}_2$  [Fig. 6(c)], we found that in contrast to  $\text{Bi}_2\text{Te}_2\text{I}_2$  where along with a sharp decrease in the value of the gap, the oscillating behavior of  $\mathbb{Z}_2$  with the num-

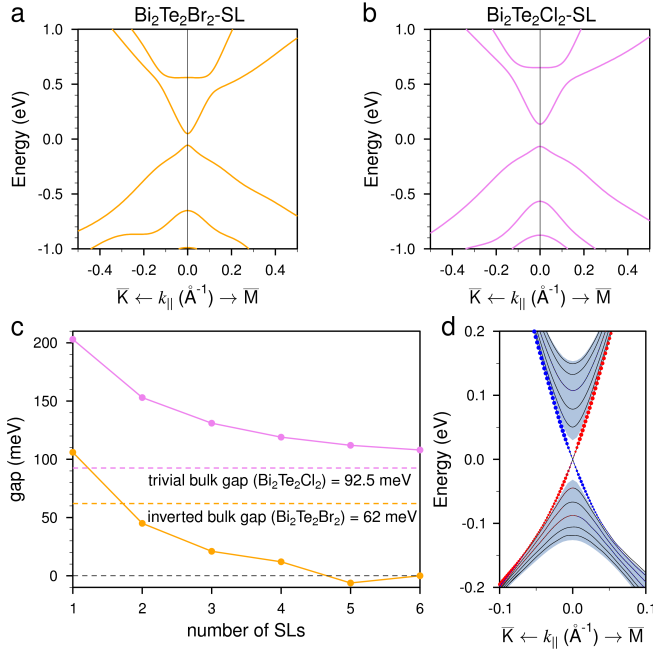


FIG. 6. Band spectra of free-standing  $\text{Bi}_2\text{Te}_2\text{Br}_2$  (a) and  $\text{Bi}_2\text{Te}_2\text{Cl}_2$  (b) SLs. The dependence of the  $\bar{\Gamma}$ -gap width on the number of SLs in  $\text{Bi}_2\text{Te}_2\text{Br}_2$  and  $\text{Bi}_2\text{Te}_2\text{Cl}_2$  thin films (c). The sign of the gap is positive for topologically trivial film and negative for non-trivial one. (d) Surface electronic structure of the 3D TI  $\text{Bi}_2\text{Te}_2\text{Br}_2$ .

ber of SLs was obtained,<sup>12</sup> the  $\text{Bi}_2\text{Te}_2\text{Cl}_2$  demonstrates a smooth decrease in the gap to its bulk value, remaining at any film thickness the trivial insulator, while  $\text{Bi}_2\text{Te}_2\text{Br}_2$  at the five-SL thickness becomes a 2D TI with the small inverted gap of 6 meV. For thicker films, the gap is zero that indicates on the converged Dirac cone of the 3D TI phase. The surface spectrum of latter is shown in Fig. 6

(d).

#### IV. CONCLUSIONS

In summary, by using first-principles calculations we have examined the topologically protected edge states and topologically trivial Rashba-split spin-polarized dangling bond states emerged at the different edges of the 2D topological insulator  $\text{Bi}_2\text{Te}_2\text{I}_2$  of one-sextuple-layer thickness. We have revealed that irrespective of the edge plane the dangling bond states lie rather far from the 2D band projected gap energy region, where the  $\bar{\Gamma}$  Dirac state resides. We also suggested the appropriate substrate for 2D  $\text{Bi}_2\text{Te}_2\text{I}_2$  QSHI, which is parental non-centrosymmetric  $\text{BiTeI}$  compound. This substrate guarantees the absence of both lattice mismatch and interface charge transfer effects. Since  $\text{BiTeI}$  is the material with the giant Rashba-type spin splitting, it produces a sizable spin splitting in 2D band structure of QSHI film. However, despite the Rashba splitting in the states forming the gap the latter remains inverted, and the 2D topological phase survives in  $\text{Bi}_2\text{Te}_2\text{I}_2/\text{BiTeI}$  heterostructure as confirmed from the  $\mathbb{Z}_2$  index calculation. We also systematically examined the possibility of realizing nontrivial 2D and 3D topological phases in thin films and bulk crystals of related hypothetical compounds composed of centrosymmetric sextuple layers of  $\text{BiTeBr}$  and  $\text{BiTeCl}$ . We have revealed that ultra thin centrosymmetric films of  $\text{Bi}_2\text{Te}_2\text{Br}_2$  are trivial band insulators up to five-SL thickness, and in the 3D limit  $\text{Bi}_2\text{Te}_2\text{Br}_2$  is a strong TI, while both 2D and 3D phases of  $\text{Bi}_2\text{Te}_2\text{Cl}_2$  are topologically trivial. We hope that our study will motivate further experimental works on topologically non-trivial centrosymmetric  $\text{BiTeX}$  systems.

This work was supported by the Spanish Ministry of Economy and Competitiveness MINECO (Project No. FIS2016-76617-P) and Saint Petersburg State University (Grant No. 15.61.202.2015).

- <sup>1</sup> C.L. Kane, and E.J. Mele,  $\mathbb{Z}_2$  topological order and the quantum spin Hall effect Phys. Rev. Lett. **95**, 146802 (2005).
- <sup>2</sup> B.A. Bernevig, and S.-C. Zhang, Quantum spin Hall effect Phys. Rev. Lett. **96**, 106802 (2006).
- <sup>3</sup> B.A. Bernevig, T.L. Hughes, and S.-C. Zhang, Quantum spin Hall effect and topological phase transition in  $\text{HgTe}$  quantum wells Science **314**, 1757 (2006).
- <sup>4</sup> M. König, S. Wiedmann, C. Brüne, A. Roth, H. Buhmann, L.W. Molenkamp, X.L. Qi, and S.-C. Zhang, Quantum spin Hall insulator state in  $\text{HgTe}$  quantum wells Science **318**, 766 (2007).
- <sup>5</sup> I. Knez, R.-R. Du, and G. Sullivan, Evidence for Helical Edge Modes in Inverted  $\text{InAs}/\text{GaSb}$  Quantum Wells, Phys. Rev. Lett. **107**, 136603 (2011).
- <sup>6</sup> Y. Ren, Z. Qiao, and Q. Niu, Topological phases in two-dimensional materials: a review Rep. Prog. Phys. **79**,

066501 (2016).

- <sup>7</sup> I.K. Drozdov, A. Alexandradinata, S. Jeon, S. Nadj-Perge, H. Ji, R.J. Cava, B. Bernevig, and Ali Yazdani, One-dimensional topological edge states of bismuth bilayers Nature Physics **10**, 664 (2014).
- <sup>8</sup> Y. Lu, W. Xu, M. Zeng, G. Yao, L. Shen, M. Yang, Z. Luo, F. Pan, K. Wu, T. Das, P. He, J. Jiang, J. Martin, Y.P. Feng, H. Lin, and X.-s. Wang, Topological Properties Determined by Atomic Buckling in Self-Assembled Ultrathin  $\text{Bi}(110)$  Nano Lett. **15**, 80 (2015).
- <sup>9</sup> Sung Hwan Kim, Kyung-Hwan Jin, Joonbum Park, Jun Sung Kim, Seung-Hoon Jhi, and Han Woong Yeom, Topological phase transition and quantum spin Hall edge states of antimony few layers, Sci. Rep. **6**, 33193 (2016).
- <sup>10</sup> Xiang-Bing Li, Wen-Kai Huang, Yang-Yang Lv, Kai-Wen Zhang, Chao-Long Yang, Bin-Bin Zhang, Y. B. Chen, Shu-Hua Yao, Jian Zhou, Ming-Hui Lu, Li Sheng, Shao-Chun

- Li, Jin-Feng Jia, Qi-Kun Xue, Yan-Feng Chen, and Ding-Yu Xing, *Experimental Observation of Topological Edge States at the Surface Step Edge of the Topological Insulator  $\text{ZrTe}_5$* , Phys. Rev. Lett. **116**, 176803 (2016).
- <sup>11</sup> R. Wu, J.-Z. Ma, S.-M. Nie, L.-X. Zhao, X. Huang, J.-X. Yin, B.-B. Fu, P. Richard, G.-F. Chen, Z. Fang, X. Dai, H.-M. Weng, T. Qian, H. Ding, and S. H. Pan, *Evidence for Topological Edge States in a Large Energy Gap near the Step Edges on the Surface of  $\text{ZrTe}_5$* , Phys. Rev. X **6**, 021017 (2016).
- <sup>12</sup> I.A. Nechaev, S.V. Eremeev, E.E. Krasovskii, P.M. Echenique, and E.V. Chulkov, *Quantum spin Hall insulators in centrosymmetric thin films composed from topologically trivial  $\text{BiTeI}$  trilayers* Sci. Rep. **7**, 43666 (2017).
- <sup>13</sup> K. Ishizaka, M. S. Bahramy, H. Murakawa, M. Sakano, T. Shimojima, T. Sonobe, K. Koizumi, S. Shin, H. Miyahara, A. Kimura, K. Miyamoto, T. Okuda, H. Namatame, M. Taniguchi, R. Arita, N. Nagaosa, K. Kobayashi, Y. Murakami, R. Kumai, Y. Kaneko, Y. Onose and Y. Tokura, *Giant Rashba-type spin splitting in bulk  $\text{BiTeI}$* , Nature Mater. **10**, 521 (2011).
- <sup>14</sup> S. V. Eremeev, I. A. Nechaev, Yu. M. Koroteev, P. M. Echenique, and E. V. Chulkov, *Ideal two-Dimensional electron systems with a giant Rashba-type spin splitting in real materials: surfaces of bismuth tellurohalides*, Phys. Rev. Lett. **108**, 246802 (2012).
- <sup>15</sup> A. Crepaldi, L. Moreschini, G. Autès, C. Tournier-Colletta, S. Moser, N. Virk, H. Berger, Ph. Bugnon, Y. J. Chang, K. Kern, A. Bostwick, E. Rotenberg, O. V. Yazyev, and M. Grioni, *Giant Ambipolar Rashba Effect in the Semiconductor  $\text{BiTeI}$* , Phys. Rev. Lett. **109**, 096803 (2012).
- <sup>16</sup> G. Landolt, S.V. Eremeev, Yu.M. Koroteev, B. Slomski, S. Muff, T. Neupert, M. Kobayashi, V.N. Strocov, T. Schmitt, Z.S. Aliev, M.B. Babanly, I.R. Amiraslanov, E.V. Chulkov, J. Osterwalder, and J.H. Dil, *Disentanglement of Surface and Bulk Rashba Spin Splittings in Noncentrosymmetric  $\text{BiTeI}$*  Phys. Rev. Lett. **109**, 116403 (2012).
- <sup>17</sup> S.V. Eremeev, I.A. Nechaev, and E.V. Chulkov, *Giant Rashba-type spin splitting at polar surfaces of  $\text{BiTeI}$*  JETP Lett. **96**, 437 (2012).
- <sup>18</sup> S.V. Eremeev, I.P. Rusinov, I.A. Nechaev, and E.V. Chulkov, *Rashba split surface states in  $\text{BiTeBr}$*  New J. Phys. **15**, 075015 (2013).
- <sup>19</sup> G. Landolt, S.V. Eremeev, O.E. Tereshchenko, S. Muff, B. Slomski, K.A. Kokh, M. Kobayashi, T. Schmitt, V.N. Strocov, J. Osterwalder, E.V. Chulkov, and J.H. Dil, *Bulk and surface Rashba splitting in single termination  $\text{BiTeCl}$*  New J. Phys. **15**, 085022 (2013).
- <sup>20</sup> M. Sakano, M. S. Bahramy, A. Katayama, T. Shimojima, H. Murakawa, Y. Kaneko, W. Malaeb, S. Shin, K. Ono, H. Kumigashira, R. Arita, N. Nagaosa, H. Y. Hwang, Y. Tokura, and K. Ishizaka, *Strongly Spin-Orbit Coupled Two-Dimensional Electron Gas Emerging near the Surface of Polar Semiconductors* Phys. Rev. Lett. **110**, 107204 (2013).
- <sup>21</sup> I.P. Rusinov, I.A. Nechaev, S.V. Eremeev, C. Friedrich, S. Blügel, and E. V. Chulkov, *Many-body effects on the Rashba-type spin splitting in bulk bismuth tellurohalides* Phys. Rev. B **87**, 205103 (2013).
- <sup>22</sup> J. Mauchain, Y. Ohtsubo, M. Hajlaoui, E. Papalazarou, M. Marsi, A. Taleb-Ibrahimi, J. Faure, K. A. Kokh, O. E. Tereshchenko, S.V. Eremeev, E.V. Chulkov, and L. Perfetti, *Circular Dichroism and Superdiffusive Transport at the Surface of  $\text{BiTeI}$* , Phys. Rev. Lett. **111**, 126603 (2013).
- <sup>23</sup> C.J. Butler, H.-H. Yang, J.-Y. Hong, S.-H. Hsu, R. Sankar, C.-I. Lu, H.-Y. Lu, K.-H. O. Yang, H.-W. Shiu, C.-H. Chen, C.-C. Kaun, G.-J. Shu, F.-C. Chou, and M.-T. Lin, *Mapping polarization induced surface band bending on the Rashba semiconductor  $\text{BiTeI}$*  Nature Commun. **5**, 4066 (2014).
- <sup>24</sup> C. Tournier-Colletta, G. Autès, B. Kierren, Ph. Bugnon, H. Berger, Y. Fagot-Revurat, O.V. Yazyev, M. Grioni, and D. Malterre, *Atomic and electronic structure of a Rashba pn junction at the  $\text{BiTeI}$  surface* Phys. Rev. B **89**, 085402 (2014).
- <sup>25</sup> M. K. Tran, J. Levallois, P. Lerch, J. Teyssier, A. B. Kuzmenko, G. Autès, O. V. Yazyev, A. Ubaldini, E. Giannini, D. van der Marel, and A. Akrap, *Infrared- and Raman-Spectroscopy Measurements of a Transition in the Crystal Structure and a Closing of the Energy Gap of  $\text{BiTeI}$  under Pressure*, Phys. Rev. Lett. **112**, 047402 (2014).
- <sup>26</sup> Sebastian Fiedler, Lydia El-Kareh, Sergey V. Eremeev, Oleg E. Tereshchenko, Christoph Seibel, Peter Lutz, Konstantin A. Kokh, Evgueni V. Chulkov, Tatyana V. Kuznetsova, Vladimir I. Grebennikov, Hendrik Bentmann, Matthias Bode and Friedrich Reinert, *Defect and structural imperfection effects on the electronic properties of  $\text{BiTeI}$  surfaces*, New J. Phys. **16**, 075013 (2014).
- <sup>27</sup> S. Fiedler, T. Bathon, S.V. Eremeev, O.E. Tereshchenko, K.A. Kokh, E.V. Chulkov, P. Sessi, H. Bentmann, M. Bode, and F. Reinert, *Termination-dependent surface properties in the giant-Rashba semiconductors  $\text{BiTeX}$  ( $X = \text{Cl}, \text{Br}, \text{I}$ )* Phys. Rev. B **92**, 235430 (2015).
- <sup>28</sup> I. P. Rusinov, T. V. Menshchikova, I. Yu. Sklyadneva, R. Heid, K.-P. Bohnen and E. V. Chulkov, *Pressure effects on crystal and electronic structure of bismuth tellurohalides*, New J. Phys. **18**, 113003 (2016).
- <sup>29</sup> H. Maaß, H. Bentmann, C. Seibel, C. Tusche, S. V. Eremeev, T. R. F. Peixoto, O. E. Tereshchenko, K. A. Kokh, E. V. Chulkov, J. Kirschner, and F. Reinert, *Spin-texture inversion in the giant Rashba semiconductor  $\text{BiTeI}$*  Nature Commun. **7**, 11621 (2016).
- <sup>30</sup> S.V. Eremeev, S.S. Tsirkin, I.A. Nechaev, P.M. Echenique, and E.V. Chulkov, *New generation of two-dimensional spintronic systems realized by coupling of Rashba and Dirac fermions*, Sci. Rep. **5**, 12819 (2015).
- <sup>31</sup> G. Bihlmayer, Yu. M. Koroteev, T. V. Menshchikova, E. V. Chulkov, and Stefan Blügel, *Ab Initio Calculations of Two-Dimensional Topological Insulators in Topological Insulators, Fundamentals and Perspectives* (Wiley-VCH Verlag GmbH & Co. KGaA, Weinheim, 2015).
- <sup>32</sup> T. Förster, P. Krüger, and M. Rohlfing, *Two-dimensional topological phases and electronic spectrum of  $\text{Bi}_2\text{Se}_3$  thin films from GW calculations*, Phys. Rev. B **92**, 201404(R) (2015).
- <sup>33</sup> T. Förster, P. Krüger, and M. Rohlfing, *GW calculations for  $\text{Bi}_2\text{Te}_3$  and  $\text{Sb}_2\text{Te}_3$  thin films: Electronic and topological properties*, Phys. Rev. B **93**, 205442 (2016).
- <sup>34</sup> I. A. Nechaev and E. E. Krasovskii, *Relativistic k-p Hamiltonians for centrosymmetric topological insulators from ab initio wave functions*, Phys. Rev. B **94**, 201410 (2016).
- <sup>35</sup> V. N. Menshov, V. V. Tugushev, and E. V. Chulkov, *Spin Hall Conductivity in Three-Dimensional Topological Insulator/Normal Insulator Heterostructures*, JETP Letters **102**, 754 (2015).
- <sup>36</sup> A. Takayama, T. Sato, S. Souma, T. Oguchi, and T. Takahashi, *One-Dimensional Edge States with Giant Spin Splitting in a Bismuth Thin Film* Phys. Rev. Lett. **114**, 066402 (2015).



- (2015).
- <sup>37</sup> T. Hirahara, G. Bihlmayer, Y. Sakamoto, M. Yamada, H. Miyazaki, S.-i. Kimura, S. Blügel, and S. Hasegawa, *Interfacing 2D and 3D Topological Insulators: Bi(111) Bilayer on Bi<sub>2</sub>Te<sub>3</sub>* Phys. Rev. Lett. **107**, 166801 (2011).
  - <sup>38</sup> F.-C. Chuang, L.-Z. Yao, Z.-Q. Huang, Y.-T. Liu, C.-H. Hsu, T. Das, H. Lin, and A. Bansil, *Prediction of Large-Gap Two-Dimensional Topological Insulators Consisting of Bilayers of Group III Elements with Bi* Nano Lett. **14**, 2505 (2014).
  - <sup>39</sup> M. Zhou, W. Ming, Z. Liu, Z. Wang, P. Li, and F. Liu, *Epitaxial growth of large-gap quantum spin Hall insulator on semiconductor surface* Proc. Natl Acad. Sci. **111**, 14378 (2014).
  - <sup>40</sup> M. Zhou, W. Ming, Z. Liu, Z. Wang, Y. Yao and F. Liu, *Formation of quantum spin Hall state on Si surface and energy gap scaling with strength of spin orbit coupling* Sci. Rep. **4**, 7102 (2014).
  - <sup>41</sup> C.-H. Hsu, Z.-Q. Huang, F.-C. Chuang, C.-C. Kuo, Y.-T. Liu, H. Lin, and A. Bansil, *The nontrivial electronic structure of Bi/Sb honeycombs on SiC(0001)* New J. Phys. **17**, 025005 (2015).
  - <sup>42</sup> Z.-Q. Huang, B.-H. Chou, C.-H. Hsu, F.-C. Chuang, H. Lin, and A. Bansil, *Tunable topological electronic structure of silicene on a semiconducting Bi/Si(111)- $\sqrt{3} \times \sqrt{3}$  substrate* Phys. Rev. B **90**, 245433 (2014).
  - <sup>43</sup> Z.-Q. Huang, F.-C. Chuang, C.-H. Hsu, Y.-T. Liu, H.-R. Chang, H. Lin, and A. Bansil, *Nontrivial topological electronic structures in a single Bi(111) bilayer on different substrates: a first-principles study* Phys. Rev. B **88**, 165301 (2013).
  - <sup>44</sup> Z. Song, C.-C. Liu, J. Yang, J. Han, M. Ye, B. Fu, Y. Yang, Q. Niu, J. Lu, and Y. Yao, *Quantum spin Hall insulators and quantum valley Hall insulators of BiX/SbX (X=H, F, Cl and Br) monolayers with a record bulk band gap* NPG Asia Materials **6**, e147 (2014).
  - <sup>45</sup> F.-C. Chuang, C.-H. Hsu, H.-L. Chou, C.P. Crisostomo, Z.-Q. Huang, S.-Y. Wu, C.-C. Kuo, W.-C. V. Yeh, H. Lin, and A. Bansil, *Prediction of two-dimensional topological insulator by forming a surface alloy on Au/Si(111) substrate* Phys. Rev. B **93**, 035429 (2016).
  - <sup>46</sup> P.E. Blöchl, *Projector augmented-wave method*, Phys. Rev. B **50**, 17953 (1994).
  - <sup>47</sup> G. Kresse, D. Joubert, *From ultrasoft pseudopotentials to the projector augmented-wave method*, Phys. Rev. B **59**, 1758 (1999).
  - <sup>48</sup> G. Kresse, J. Hafner, *Ab initio molecular dynamics for open-shell transition metals*, Phys. Rev. B **48**, 13115 (1993).
  - <sup>49</sup> G. Kresse, J. Furthmüller, *Efficient iterative schemes for ab initio total-energy calculations using a plane-wave basis set*, Phys. Rev. B **54**, 11169 (1996).
  - <sup>50</sup> S. Grimme, J. Antony, S. Ehrlich, and H. Krieg, *A consistent and accurate ab initio parametrization of density functional dispersion correction (DFT-D) for the 94 elements H-Pu*, J. Chem. Phys. **132**, 154104 (2010).
  - <sup>51</sup> A.A. Soluyanov, and D. Vanderbilt, *Computing topological invariants without inversion symmetry* Phys. Rev. B **83**, 235401 (2011).
  - <sup>52</sup> Jacob Linder, Takehito Yokoyama, and Asle Sudbø, *Anomalous finite size effects on surface states in the topological insulator Bi<sub>2</sub>Se<sub>3</sub>*, Phys. Rev. B **80**, 205401 (2009).
  - <sup>53</sup> N. Virk, and O.V. Yazyev, *Dirac fermions at high-index surfaces of bismuth chalcogenide topological insulator nanostructures* Sci. Rep. **6**, 20220 (2016).